

KISHIN MOORJANI, FRANK J. ADRIAN, BORIS F. KIM, JOSEPH BOHANDY, TERRY E. PHILLIPS, THOMAS J. KISTENMACHER, WILLIAM J. GREEN, ELISABETTA AGOSTINELLI, BRADLEY G. BOONE, and RAY M. SOVA

HIGH-TEMPERATURE SUPERCONDUCTIVITY

The second stage of APL's continuing program on high-temperature superconductors, including recent advances, is reviewed. Present emphasis is on producing the high quality samples needed for current experiments and envisioned devices, development of novel methods for judging sample quality, and device concepts using various novel structural features of the cuprate oxide superconductors, such as their intrinsic Josephson junctions. Additionally, some theoretical investigations and the interplay of superconductivity and magnetism in high-temperature superconductors are discussed.

INTRODUCTION

High-temperature superconductivity based on oxide materials was developed less than three years ago. The initial "hype" that accompanied the discovery of superconductivity at temperatures above the boiling point of liquid nitrogen must now be replaced with realistic assessments of what can be achieved with the new materials, and what their limitations may be. Progress toward that goal is being made continuously. The excitement is still present, although it has been largely transformed from popular media to the scientific literature and conferences, so as to allow researchers to calmly conduct the task of evaluating and understanding the fascinating behavior of superconducting oxides.

The highest confirmed value of the superconducting transition temperature, T_c , remains at 125 K for the thallium-based oxides, though tantalizing reports of values of T_c almost twice as large emerge periodically. The latter values, however, have never been widely reproduced and must therefore be considered unconfirmed. It should be emphasized that the confirmed values of T_c represent highly satisfactory materials for devices operating at 77 K. In this regard, elevated values of critical currents (greater than 5×10^6 A/cm²) are now routinely observed in thin-film samples of various oxides, making possible the initial exploitation of superconductors in small-scale applications. Since semiconducting devices operate quite efficiently at 77 K, there now exists an overlapping temperature region for semiconductor devices and superconducting thin films that can be exploited for hybrid devices.

Device structures for hybrid microelectronics, however, pose their own constraints.¹ Among them are the cost-effectiveness of thin- and thick-film processing techniques that can be employed to form mechanically and

thermally stable structures on technologically useful substrates at low processing temperatures. Furthermore, normal metal contacts to superconducting oxides need to be formed and it is imperative that the device structures be able to withstand exposure to the ambient environment without degradation of their performance. Certain applications require patterned film structures, and once again the deleterious effects of patterning techniques must be minimized. For complete characterization of layers, it is essential not to rely only on standard measurements (for example, the temperature-dependence of the resistivity), but to develop novel methods to probe globally the characteristics of films and the structures based on them. Buffer layers to enhance superconducting behavior and passivation layers to guard against degradation are other important areas. Finally, the ubiquitous anisotropic crystal structure and properties of all the high-temperature superconducting ceramics discovered to date demand fabrication of films with preferred orientation. Every superconducting ceramic system exhibits its own peculiarities; while the properties of compounds based on rare earths are sensitive to the ambient environment, the bismuth-based materials are mechanically fragile and the thallium-based samples need careful handling because of their toxicity.

Perhaps the most important aspect of superconducting oxides—their theoretical understanding—remains an unachieved goal. The design of new materials with higher values of T_c is, therefore, necessarily an empirical path.

In this article, we discuss the considerable progress on high-temperature superconductors achieved at APL since our last *Technical Digest* article on the subject.² It covers the entire range from materials studies and thin-layer formation to the design of novel techniques for their in-

vestigation, theoretical modeling, and device concepts. The details of our research are contained in more than 50 articles, two patents, and five invention disclosures.

LASER ABLATION PROCESSING

Laser ablation processing (LAP) of superconducting materials has been demonstrated to lead to proper stoichiometry for superconducting films from a single target.³ The method, first exploited by APL, is clean and cheap and has become the technique of choice in many laboratories around the world. We have now designed a custom vacuum cell to upscale and automate the process for increased throughput.

This cell incorporates target and substrate carousels, each holding six specimens. One of the substrate carousel positions has a heater and cooler for controlling the substrate temperature. Each carousel has three orthogonal translational degrees of freedom, two of which are in the plane of the carousel. The in-plane translations are controlled by a computer via micromanipulators driven by stepper motors. This motion allows uniform depositions on the substrate, and uniform ablation from the target (Fig. 1).

Software has been written to control the motion of the target and substrate during deposition. This program depicts graphically, in real time, the positions of the laser spot on the target and the deposition on the substrate. The ablation history of the target is stored in a file for future reference. At present, the laser is run asynchronously, with its own internal clock. Future hardware development is planned, so that the laser can be fired by the computer.

The LAP technique has been employed to deposit thin films of La-Sr-Cu-O, Y-Ba-Cu-O, and Bi-Sr-Ca-Cu-O.²⁻⁵ A thin film of the latter composition has also been chemically etched to obtain a meander-line structure (Fig. 2) that is presently being investigated for the development of a radiation sensor.

Despite the many advantages of the LAP technique, its principal disadvantage is the so-called "splashing effect"—the splashing onto the substrate surface of microscopic particles from the target, which can seriously deteriorate the quality of the film. To overcome that hurdle, we have deposited films from a melt-quenched amorphous target, which has higher density and uniformity than the sintered targets, and we have demonstrated that the resulting films have only 10% of the particulate matter on surfaces, as compared to the films obtained from sintered targets.⁶ This should prove extremely important in eventual formation of films with smooth surfaces that are essential in forming multilayers either of superconducting materials with varying T_c , or in hybridized devices employing superconductors and nonsuperconductors. Further research in this area is in progress.

MODULATED TECHNIQUES FOR STUDYING SUPERCONDUCTORS

The resistance, R , of a superconducting sample can be functionally written as $R = R(\omega, Q)$ to reflect its dependence on the frequency, ω , at which the measure-

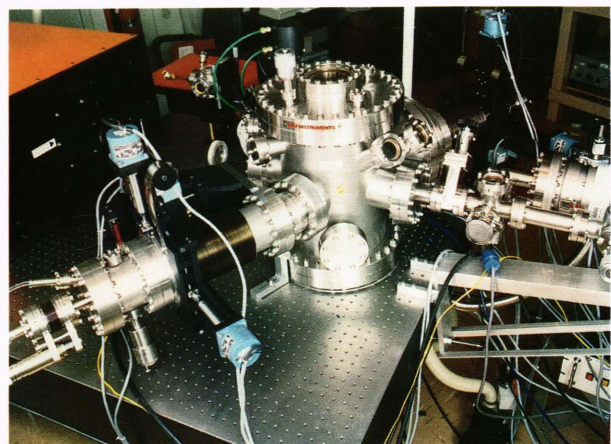


Figure 1. Upscaled and automated laser ablation processing cell used to form thin-layer structures.

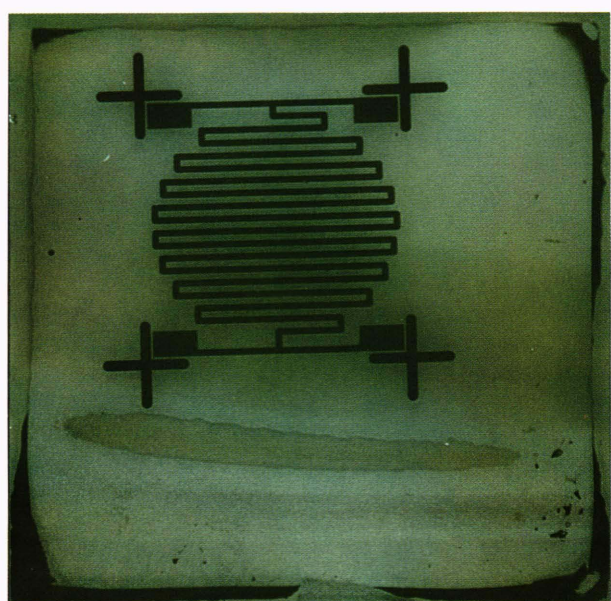


Figure 2. BSCCO meander-line element with overall dimensions of 0.2×0.2 in. and a line width of 0.005 in. The element was patterned using wet chemistry etching. Further reductions in the size of the element will be required to optimize performance.

ment is made and on a set of independent parameters, Q , that include temperature, external magnetic field, etc. Consequently, the modulation of the independent parameters induces corresponding modulation of the resistance so that for small modulations in R , one can write

$$R(\omega, Q) = R(\omega, Q_0) + \sum \left(\frac{\partial R}{\partial Q_i} \right)_{Q_0} \delta Q_i ,$$

where Q_0 denotes a set of time-independent values of the parameters Q , and δQ_i is the value of the i th parameter that is modulated. One therefore has a possibility of a set of techniques for investigating superconductors, depending on which particular parameter, or

combination of them, is modulated. Previously, we have extensively exploited the method at microwave frequencies in the magnetically modulated microwave absorption (MAMMA) technique,^{2,7-9} which has the advantage that it can be employed to study electrically discontinuous samples (such as powders, discontinuous films, etc.).

The basic principle of the MAMMA method (an increasing magnetic field decreases T_c) does not depend on the presence of microwaves or microwave absorption in the sample. Therefore, we expect that this technique can be used in conjunction with any means of measuring loss in superconducting samples, including DC resistance. We have recently demonstrated this by a magnetically modulated electrical resistance (MAMER) technique¹⁰⁻¹² for detecting superconductivity. The scope of magnetic modulation methods to detect and study superconductivity is thus enlarged to include a simpler MAMER configuration in samples that are electrically continuous.

The method was first tested on a thin-film sample of the conventional superconductor NbN. Figures 3A and 3B show the DC resistance and the MAMER response, respectively, simultaneously recorded as a function of temperature using 5-G magnetic field modulation, H_{mod} , and a 30-G DC magnetic field, H_{DC} . The superconducting transition at about 15 K is extremely sharp (about 0.2 K) and one sees that the MAMER response is, indeed, approximately proportional to the derivative of the DC resistance with respect to temperature, as expected from a qualitative model of this method for the MAMMA case.⁷

The utility of the MAMER technique for a superconducting oxide is shown in Figure 4 for a $\text{EuBa}_2\text{Cu}_3\text{O}_{7-y}$ bulk sample, and the corresponding MAMMA response is shown in Figure 5. Both techniques provide a simple method for studying the effect of increasing field on T_c .

and also for studying the effect of inherent anisotropy of these materials. An example of the latter is presented in Figure 6, which shows the MAMMA spectrum and the simultaneously recorded unmodulated microwave resistance of a Y-Ba-Cu-O crystal with a 30-G DC magnetic field parallel to the c -axis.¹³ The microwave resistance is increasing with decreasing temperature down to 87 K, at which temperature the resistance drops and a MAMMA peak is observed at 86 K. In addition, one sees that there is a second superconducting phase in the crystal, with a transition temperature around 81 K. Additional measurements show that there is more than one additional phase present.

Any magnetic anisotropy that may exist in the sample can be investigated using this technique by obtaining MAMMA spectra as a function of the direction of the DC magnetic field with respect to the different crystallographic axes of the crystal. MAMMA spectra were obtained with the magnetic field in each of three crystallographic planes; Figure 7 shows representative spectra of the YBCO crystal with the magnetic field along the three crystallographic axes.

The edges of the rectangularly shaped crystal platelet were arbitrarily labeled a and b since twinning precludes the assignment of specific crystallographic axes to the in-plane directions.

The MAMMA spectra with $H \parallel c$ and $H \parallel b$ (Figs. 7A and 7B, respectively) are representative of all the spectra in the $a-c$ and $b-c$ planes. There are clearly two different phases, separated by 5 K. Furthermore, some of the spectra in these two planes indicate the existence of a very small amount of a third superconducting phase in the vicinity of 68 to 70 K. The direction of H has a relatively small effect on the position of the peaks, producing shifts in the values of T_c up to approximately 2 K.

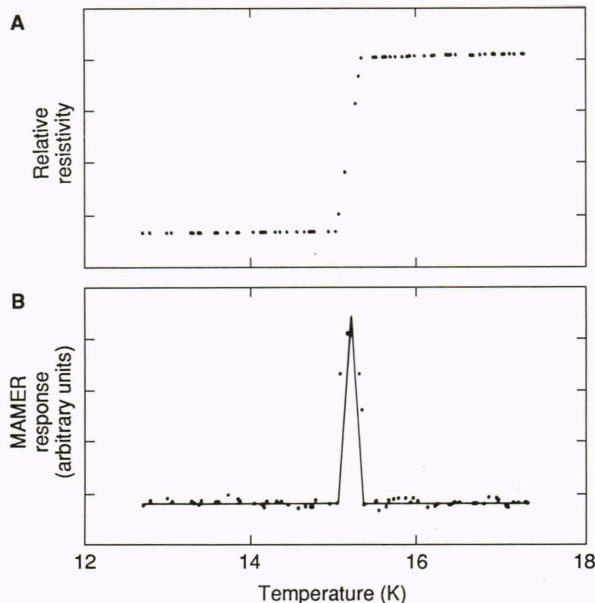


Figure 3. A. The DC resistance and B the magnetically modulated electrical resistance of a thin film of NbN as a function of temperature. ($H_{\text{DC}} = 30$ G, $H_{\text{mod}} = 5$ G, and $I = 100$ μA .)

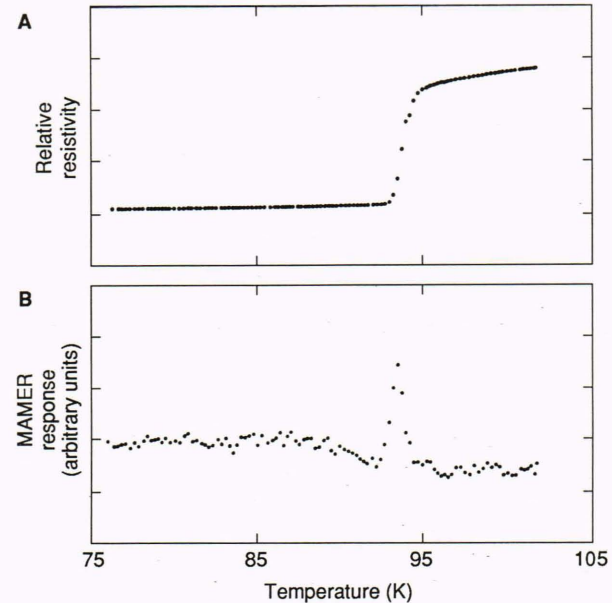


Figure 4. A. The DC resistance and B the magnetically modulated electrical resistance of $\text{EuBa}_2\text{Cu}_3\text{O}_{7-y}$ as a function of temperature. ($H_{\text{DC}} = 1$ kG, $H_{\text{mod}} = 5$ G, and $I = 5$ mA.)

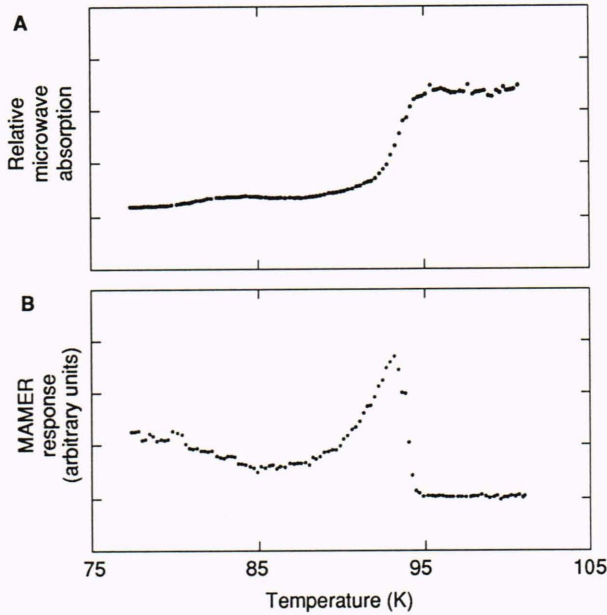


Figure 5. **A.** The unmodulated microwave absorption and **B** the magnetically modulated microwave absorption of $\text{EuBa}_2\text{Cu}_3\text{O}_{7-y}$. ($H_{\text{DC}} = 1 \text{ kG}$ and $H_{\text{mod}} = 2 \text{ G}$.)

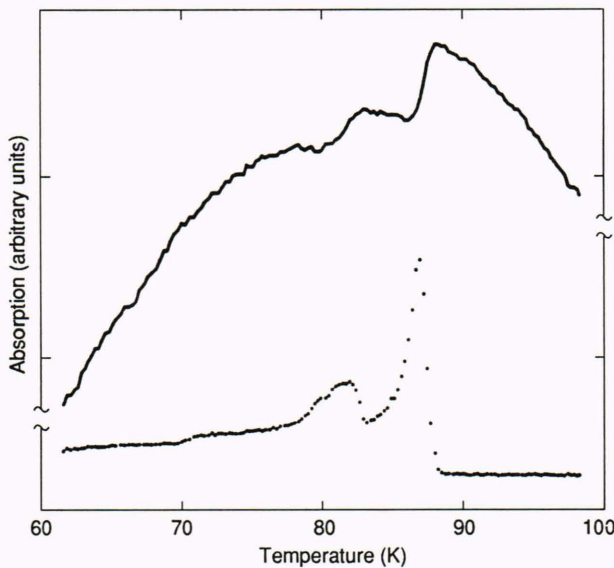


Figure 6. The unmodulated microwave absorption (upper curve) and the magnetically modulated microwave absorption (lower curve) of the Y-Ba-Cu-O crystal. ($H_{\text{DC}} = 30 \text{ G}$, parallel to the c -axis).

For the in-plane orientation of Figure 7B, the MAMMA spectrum is very similar to the $H \parallel c$ spectrum, although the intensity of the $H \parallel c$ spectrum is about 6 times stronger. This is likely because the MAMMA response is proportional to dT_c/dH , and $|dT_c/dH|_{H \parallel c} > |dT_c/dH|_{H \perp c}$ in these materials. However, when H is in the $a-b$ plane (Fig. 7C) a dramatic change occurs in the MAMMA spectrum. The two peaks observed in the other orientations have inverted in intensity and two new

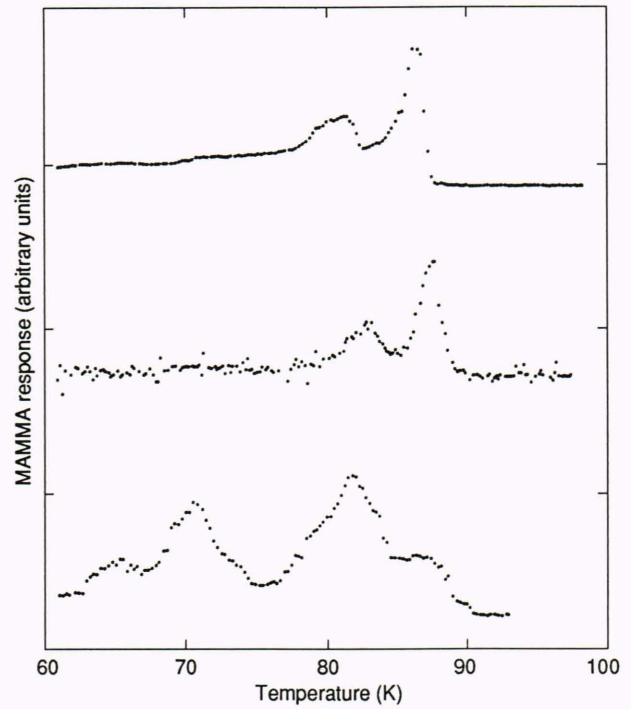


Figure 7. The orientation-dependence of the MAMMA spectra of the Y-Ba-Cu-O crystal: $H_{\text{DC}} \parallel c$, $H_{\text{RF}} \parallel a$ (upper curve); $H_{\text{DC}} \parallel b$, $H_{\text{RF}} \parallel a$ (middle curve); and $H_{\text{DC}} \parallel a$, $H_{\text{RF}} \parallel c$ (lower curve).

peaks have appeared at lower temperature. Although the origin of these effects is unknown (including whether the physically important orientation-dependence is with respect to the external magnetic field or to the microwave fields) a detailed study of this orientation dependence shows that it is consistent with and thus somehow related to crystal twinning, in which the twins are related by a 45° rotation about the c -axes. This aspect of our results is being studied in greater detail.

The MAMMA method has also been used to obtain homogenized samples of Pb-stabilized Bi-based oxide superconductors with $T_c = 108 \text{ K}$ by optimizing processing conditions.¹⁴

WEAK-LINK SUPERCONDUCTIVITY

It is clear that the large differences between (1) the critical current and its dependence on temperature and magnetic field in single crystals and ordered thin films of the high- T_c superconductors, and (2) those of composite polycrystalline samples result from different critical-current-limiting mechanisms. Single crystals of the oxide superconductors are similar to conventional type II superconductors in that in a strong magnetic field they maintain a large enough superconducting region to carry sizable currents by trapping the flux in uniformly distributed regions within the superconductor. Unfortunately, in the ceramic superconductors these trapped-flux regions are fixed or pinned only at temperatures considerably below T_c , and their motion above T_c (the flux lattice melting temperature, T_m) produces interactions

between the trapped flux and the superconducting currents that render the superconductor ineffective¹⁵ (at least for high current applications) above T_m . A manifestation of this effect is the marked tail that appears below T_c in the resistance-versus-temperature curve of single crystals of the ceramic superconductors in large magnetic fields (on the order of 1 T). On the other hand, the critical currents in bulk sintered samples consisting of a myriad of small crystalline grains are lower than those in single crystals and have a greater magnetic field dependence at low magnetic fields. These properties are generally ascribed to the presence of structural disorder (e.g., defects and dislocations) as well as compositional disorder (for example, impurities and grain boundaries) in the bulk samples, leading to the formation of weak links that control the critical current and make it strongly dependent on the magnetic field. Given the small, highly anisotropic values of the coherence lengths in superconducting ceramics, even very small-scale disorder of about 10 Å can lead to weak links. The presence of weak links of the Josephson junction type in sintered samples of $\text{YBa}_2\text{Cu}_3\text{O}_{7-y}$ was conjectured⁷ soon after these materials became available; subsequently, it was argued that the tail on the low temperature side of the resistance-versus-temperature curve of the granular superconductors is caused by weak links.¹⁶

Thus, it is important to distinguish between effects observed in granular samples, where weak-link effects are likely to predominate, and single-crystal and oriented thin-film samples, where weak links are far fewer and flux motion effects come to the fore. These dissimilar effects in the granular and single-crystal samples may even be of practical importance in optimizing the critical currents in the high- T_c superconductors because, although the critical currents are generally lower in the granular samples, the grain boundaries, dislocations, etc., may provide flux-pinning sites and thereby reduce the effects of flux motion. A compromise between perfectly ordered single crystals or thin films and highly disordered polycrystalline samples may be needed to produce high T_c superconductors capable of carrying useful currents at temperatures close to T_c . In any event, it is important to have methods capable of observing weak-link effects. Here we describe how both the MAMMA and MAMER methods clearly differentiate the response owing to the intrinsic superconducting transition within the individual crystallites of the granular sample from that of the weak links between these granules.^{12,17,18}

Figures 8A through 8D show the MAMER spectra and simultaneously recorded resistance curves of a sample of $\text{EuBa}_2\text{Cu}_3\text{O}_{7-y}$ (EBCO) in static magnetic fields of 500, 30, 10, and 2 G, respectively, using a 5-mA excitation current. The MAMER response in a 500-G field (Fig. 8A) is characterized by a derivative peak, subsequently referred to as the intrinsic peak, occurring at a temperature (T_c) at the inflection point in the resistance curve. An additional, though more subtle feature—a very broad secondary weak peak in the MAMER response—is also observed on the low temperature side of the main transition. In the $\times 10$ expansion of the resistance curve (Fig. 8A), note that there is significant tailing on the low tem-

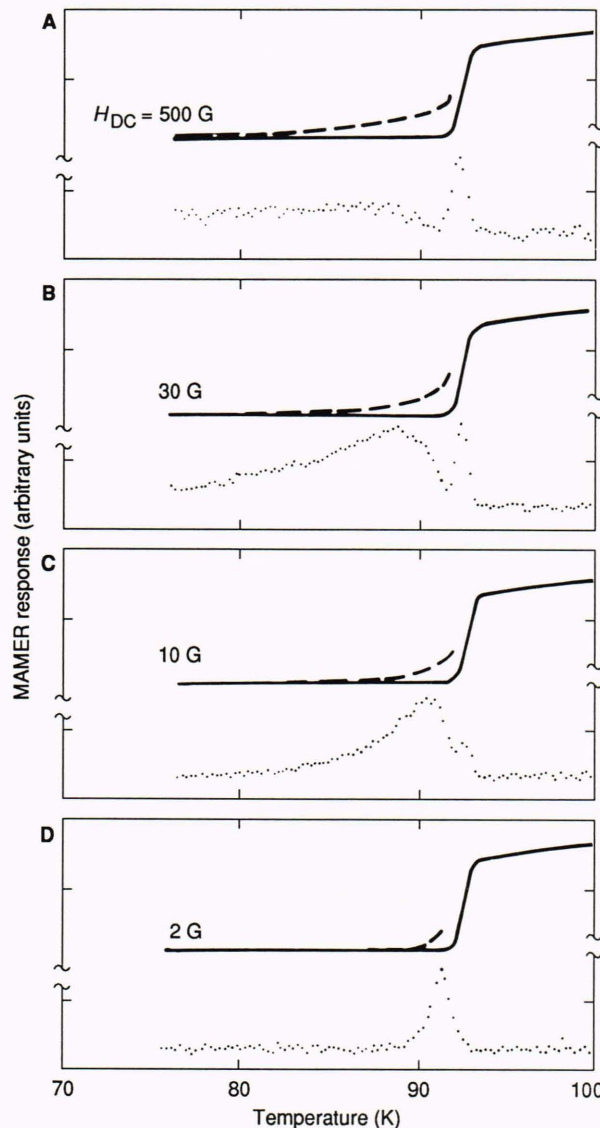


Figure 8. Magnetic field dependence of the MAMER response (dotted) and DC resistance ($\times 1$, solid; $\times 10$, dashed) of $\text{EuBa}_2\text{Cu}_3\text{O}_{7-y}$ using a current of 5 mA. (A, B, and C, 5-G modulation amplitude; D, 1-G modulation amplitude.)

perature side of the primary resistance transition. As the static field is reduced to 30 G (Fig. 8B), the resistance tail has been reduced considerably; clearly, the extent of this resistive tail depends on the magnitude of the applied magnetic field. Correspondingly, the weak peak on the low temperature side of the intrinsic MAMER peak has evolved into a broad, reasonably well-defined peak. Lowering the static field to 10 G (Fig. 8C) results in a narrowing and a shift to higher temperature of the secondary MAMER peak, effecting increased amplitude relative to the intrinsic peak and, concomitantly, a continued reduction of the resistive tail. In a 2-G static field and with 1-G modulation amplitude (Fig. 8D), the intrinsic peak is barely discernible as a weak shoulder on the secondary peak, and the tailing is further reduced.

The correlation of the secondary MAMER peak with the resistive tail, with its extreme sensitivity to small mag-

netic fields, and with the agreement with the weak-link model (to be presented later), led us to associate the secondary MAMER peak with the presence of weak links. The weak-link response dominates the intrinsic response at low magnetic fields because (as a phenomenological model will later show) the weak-link critical currents are very strongly field-dependent at low fields.

The effect of current on the MAMER spectra is seen by comparing Figure 8 (5 mA) with Figure 9 (100 mA). The height of the intrinsic peak is, as one would expect, proportional to the applied current, and both peaks shift to lower temperatures. We are primarily interested, however, in the relative behavior of the weak-link peak. It is seen from Figures 8 and 9 that the effect of current is qualitatively similar to that of a magnetic field, in that increasing the current lowers the temperature of the weak-link peak and broadens it, though it is more symmetrical. Note that, with a fixed field, the relative height of the weak-link peak with respect to the intrinsic peak is higher with the higher measuring current. This may be related to the fact that the peak obtained with the larger current is more symmetrical, the tail having moved more to the center of the peak.

We have simulated the results of the MAMER experiment, taking into account the behavior of both intrinsic and weak-link responses. (This approach also applies to the MAMMA experiment.) The temperature and magnetic field dependence of the intrinsic resistance of the bulk superconductor is conveniently represented by the empirical temperature-step function, $R_i(T,H)$, which may be expressed as

$$R_i(T,H) \sim \left\{ 1 + \exp \left[-\alpha \left(\frac{T}{T_c} - 1 + aH \right) \right] \right\}^{-1}, \quad (1)$$

where T is the temperature, H is the magnetic field, and α determines the abruptness of the superconducting phase transition.

The MAMER response is proportional to $\partial R_i / \partial H$ and is consequently an absorption-like peak located at the midpoint of the step in $R_i(T,H)$. Since the model focuses on the response from weak links, we have also ignored the current dependence of the intrinsic peak.

The resistance of a weak link is expected to increase rapidly from zero (superconducting) to a finite value as the current, I , through the link, approaches the critical current of the link, which is a function of temperature and magnetic field, $I_c(T,H)$. An empirical formula that mimics this behavior is

$$R_w(T,H) \sim \left\{ 1 + \exp \left[-\beta \left(1 - \frac{I_c(T,H)}{I} \right) \right] \right\}^{-1}, \quad (2)$$

where β is an empirical constant representing the abrupt-

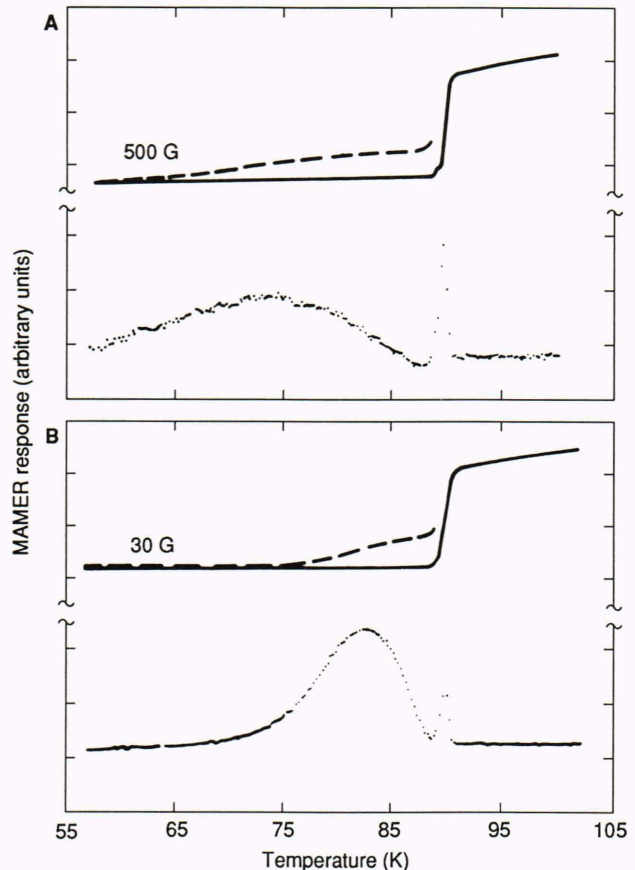


Figure 9. The MAMER response (dotted) and DC resistance ($\times 1$, solid; $\times 10$, dashed) of $\text{EuBa}_2\text{Cu}_3\text{O}_{7-y}$ using a 100-mA current and 5-G modulation amplitude. (A, $H_{DC} = 500$ G and B, $H_{DC} = 30$ G.)

ness of the weak-link superconducting transition. The corresponding MAMER response is proportional to

$$\left(\frac{\partial R_w}{\partial H} \right)_T = \left[\left(\frac{\partial R_w}{\partial I_c} \right) \left(\frac{\partial I_c}{\partial H} \right) \right]_T. \quad (3)$$

The critical current, I_c , for a single weak link is given by

$$I_c(T,H) = I_c(T,0) \frac{|\sin(\pi H/H_0)|}{\pi H/H_0}, \quad (4)$$

where H_0 is the field that provides a magnetic flux of 1 fluxon in the weak link, and $I_c(T,0)$, the critical current in the vicinity of T_c at 0 magnetic field, is reported to have the temperature-dependence¹⁹

$$I_c(T,0) = I_0 (1 - T/T_c)^2. \quad (5)$$

For a single Josephson junction, $\partial R_w / \partial H$, which determines the MAMER signal, is obtained by using Equations 4 and 5 in Equation 3 as

$$\begin{aligned} \left(\frac{\partial R_w}{\partial H} \right)_T &= \frac{\beta R_w f(I_c/I)}{1 + f(I_c/I)} \frac{I_0}{I} \\ &\times \left(1 - \frac{T}{T_c} \right)^2 \left\{ \frac{1}{H} \frac{|\sin(\pi H/H_0)|}{(\pi H/H_0)} \right. \\ &\left. - \frac{1}{H} \operatorname{sgn}[\sin(\pi H/H_0)] \cos(\pi H/H_0) \right\}, \end{aligned} \quad (6)$$

where $f(I_c/I) = \exp[\beta(I_c/I - 1)]$ and $\operatorname{sgn}(x) = 1, 0$, and -1 for $x > 0, x = 0$, and $x < 0$, respectively. Thus, the contribution of a large number of junctions with different values of H_0 smoothes out the fluctuations in the first (always positive) term, while averaging the second (purely oscillating) term to 0. The surviving term clearly decreases rapidly with external field.

We will perform the following analysis in accordance with the previous discussion. The sample is considered to consist of thin slabs stacked perpendicular to the direction of current, with each slab containing a large array of weak links in parallel, whose H_0 values are distributed according to an asymmetrical Gaussian distribution (because $H_0 > 0$). Each of these parallel arrays of weak links is serially connected with the neighboring arrays, and because the weak links are uniformly distributed, all the arrays are considered to be equivalent (the mean and variance of the Gaussian distribution of H_0 is the same in each parallel array). Although this is not strictly justified, since a distribution of means would be expected among the parallel arrays, the effect of our simplification in this regard is of secondary importance in explaining the experimental results presented here. We will discuss the consequences of this approximation later.

In terms of the above model, the resistance of the serially connected array is the same as that of a single array, aside from a constant scaling factor. Thus a single array suffices to represent the critical-current function for the entire sample. Taking the value of I_0 to be the same for all weak links, the critical weak-link current for the sample can be represented by

$$\begin{aligned} I_c(T, H) &= I_0 (1 - T/T_c)^2 N \sum_{H_0} \left\{ \frac{|\sin(\pi H/H_0)|}{\pi H/H_0} \right. \\ &\times \left. \exp \left[- \left(\frac{H_0 - H_{av}}{\sigma} \right)^2 \right] \right\}, \end{aligned} \quad (7)$$

where the factor N normalizes the summation, and H_{av} is the average field. The sum has been carried out over approximately 20,000 inequivalent junctions with H_0 randomly distributed in the range from 1 to 100 G. The values of I_0 , β , H_{av} , and σ were determined to provide a fit to the experimental data; the resulting values were $I_0 = 300$ A, $\beta = 0.5$, $H_{av} = 5$ G, and $\sigma = 30$ G.

The MAMER response, M , for the sample was simulated by taking a linear combination of the corresponding response for intrinsic and weak link material,

$$M \sim \frac{\partial R_I}{\partial H} + K \frac{\partial R_w}{\partial H}, \quad (8)$$

where the constant K was obtained from the relative intrinsic and weak-link peak heights in one of the spectra. Calculated MAMER spectra using the parameters given in the preceding paragraph along with the experimental values of current and magnetic field used in the experiments are shown in Figures 10 and 11.

A comparison of the data in Figures 8 and 9 and the corresponding calculated spectra in Figures 10 and 11 indicates that the simulation reproduces the general behavior of the weak-link peaks relative to that of the intrinsic peaks for different magnetic fields and currents. In particular, the simulation correctly reproduces the observed broadening and shift of the weak-link peaks to lower temperatures with increasing field and current. It also correctly shows that the peak height decreases with increasing field.

SUPERCONDUCTIVITY AND MAGNETISM

It has been suggested that the origin of superconductivity in superconducting oxides may be magnetic in nature.²⁰ A possibility for studying the interplay of superconductivity and magnetism in $\text{YBa}_2\text{Cu}_3\text{O}_{7-y}$ is via substitutions of various magnetic species for the non-magnetic ones in these materials. In particular, replacing Cu by Fe suppresses T_c .²¹ Several samples of the Fe-substituted perovskite series, $\text{RBa}_2(\text{Cu}_{1-x}\text{Fe}_x)_3\text{O}_{7-y}$ (with $\text{R} = \text{Y}$, Gd , or Eu , and $0 \leq x \leq 0.15$) were pre-

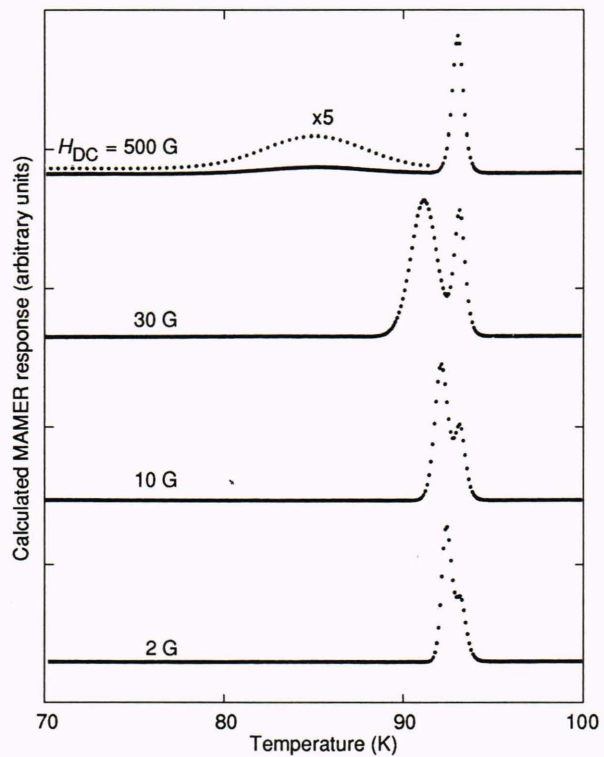


Figure 10. Calculated field dependence of the MAMER response of $\text{EuBa}_2\text{Cu}_3\text{O}_{7-y}$ using a current of 5 mA.

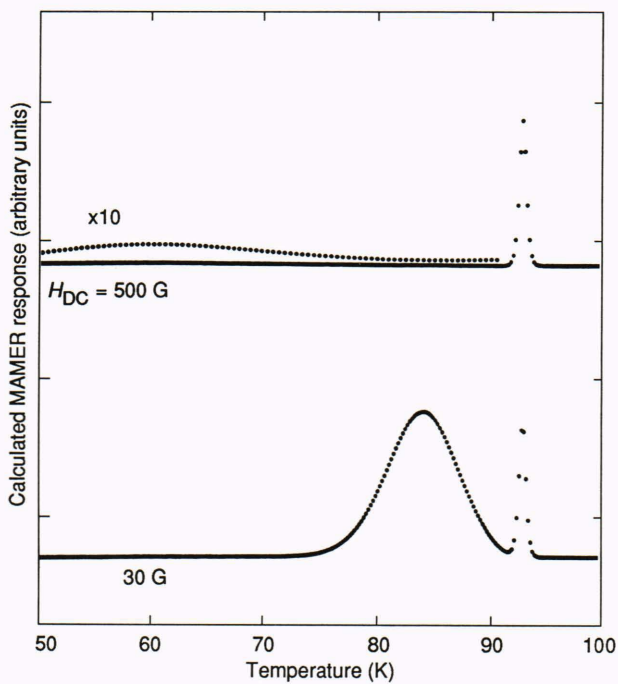


Figure 11. Calculated MAMER response of $\text{EuBa}_2\text{Cu}_3\text{O}_{7-y}$ using 100-mA current.

pared. On the basis of crystal chemistry and the ionic radii involved, Fe is expected to substitute for Cu. The substitution of Fe also has the advantage that one can investigate the local environment of Fe, and therefore of Cu, by Mössbauer spectroscopy.

The suppression of T_c with increasing Fe concentration was demonstrated by the MAMMA technique^{22,23} and the values obtained correlated well with the values obtained from the resistivity measurements.²⁴ In these samples, the room temperature Mössbauer spectra revealed two distinct Fe sites that correspond to two local oxygen coordinations of the two Cu sites which are well established from x-ray, electron, and neutron diffraction studies. Since Fe, for the most part, has clearly substituted into the Cu sites that play a central role in the superconductivity of these materials, it is rather surprising that for a concentration of Fe of 3% or greater, the Mössbauer spectra reveal magnetic ordering at 4.2 K. The spectra are complex, they show a distribution of magnetic hyperfine fields with a broad range of about 200 to 400 kOe, and they resemble those of spin glass ordering in the sense that no sharp transition to the ordered state is observed, but instead a large broadening in the wings is seen, and the spectra cannot be fitted by assuming a constant angle between the local magnetization direction and the electric field gradient.²³ The coexistence of the magnetic ordering with large local magnetization and superconductivity implies either a robust superconducting mechanism, or a rather short correlation length for electron pair formation, or both.

The nature of the magnetic ordering cannot be ascertained from the complex Mössbauer spectra and there-

fore neutron time-of-flight (TOF) measurements²⁵ were performed on the Mibemol spectrometer of the Orphée reactor in Saclay, France, with an incident wavelength of 7 Å and an instrumental resolution of 50 μeV . In the pure $\text{YBa}_2\text{Cu}_3\text{O}_{7-y}$ sample, a typical TOF spectrum is the superposition of an inelastic signal due to the phonons and of an elastic peak arising mainly from incoherent and Laue scattering. In the substituted $\text{YBa}_2(\text{Cu}_{0.88}\text{Fe}_{0.12})_3\text{O}_{7-y}$ sample, the “elastic” (resolution-limited) peak also contains a magnetic contribution from the iron spins, since its intensity is strongly temperature-dependent. In addition, we observe a quasi-elastic peak that is readily attributed to the iron spin relaxation. Focusing on the quasi-elastic and inelastic region, Figure 12 shows typical TOF spectra recorded at several temperatures for the mean q value of 0.6 \AA^{-1} . The quasi-elastic intensity increases slightly when the temperature is lowered from 122 K to about 40 K and thereafter decreases strongly with decreasing temperature. At 1.8 K no quasi-elastic intensity is detected.

The TOF spectra were fitted by a sum of a delta function (norm C_1) and a Lorentzian function (norm C_2 and energy line width Γ) converted to time scale and convoluted with experimental resolution. As shown in Figure 12, this procedure yields rather good fits. The parameters C_1 , C_2 , and Γ are shown as functions of temperature in Figure 13. The elastic intensity, C_1 , is constant between 122 K and 40 K, then starts to increase when the temperature is further reduced. Concomitantly, we observe a strong decrease of the quasi-elastic intensity, C_2 . Although the error bars are very large because of the rather poor statistical precision, a minimum of the quasi-elastic width, Γ , is suggested. This behavior of the parameters is observed independently of the q value considered.

In the $\text{YBa}_2(\text{Cu}_{0.88}\text{Fe}_{0.12})_3\text{O}_{7-y}$ sample, the changes with temperature of the fitted parameter (C_1 , C_2 , Γ) are typical of spin freezing as observed in archetypal spin glasses such as dilute CuMn or AuFe alloys.²⁶ The decrease of the quasi-elastic intensity concomitantly with the increase of the elastic intensity can be explained in a picture of spin clusters: when temperature decreases, the growing of clusters with the lowest relaxation times yields a progressive transfer from the quasi-elastic intensity to the resolution-limited or “elastic” peak. In $\text{YBa}_2(\text{Cu}_{0.88}\text{Fe}_{0.12})_3\text{O}_{7-y}$, this change occurs around 40 K, thus slightly above the freezing temperature evaluated from Mössbauer experiments (around 35 K). It should be noted that the determination of the temperature for the spin freezing depends on the experimental resolution (the time scale of the experiment is somehow shorter with the neutron probe [10^{-10} s here] than with the Mössbauer probe [10^{-7} s]).

Finally, we recall that in the $\text{YBa}_2(\text{Cu}_{0.88}\text{Fe}_{0.12})_3\text{O}_{7-y}$ sample, the freezing process and the superconductivity occur in the same temperature range (30 to 40 K). The persistence of superconductivity in spite of a noncollinear magnetic ordering implies little interaction between the superconducting and magnetic “lattice,” possibly because of the preferential occupation of the Cu(I) site by

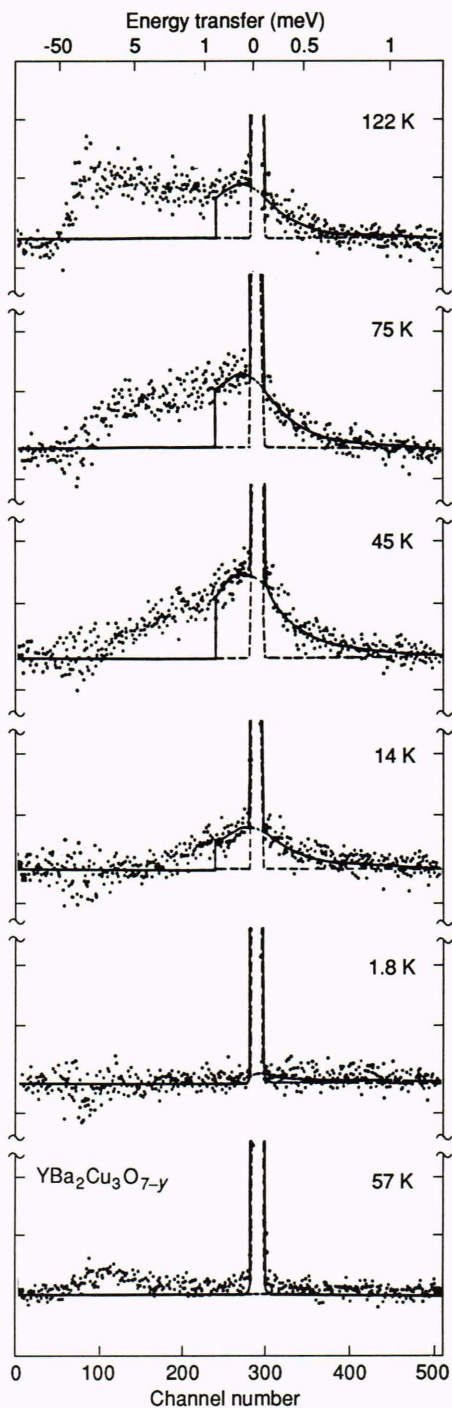


Figure 12. TOF spectra at several temperatures in $\text{YBa}_2(\text{Cu}_{0.88}\text{Fe}_{0.12})_3\text{O}_{7-y}$. The intensities have been normalized to the same number of incident neutrons. The intensity of the $\text{YBa}_2\text{Cu}_3\text{O}_{7-y}$ sample at 57 K is also shown for comparison. (Reprinted, with permission, from Ref. 25.)

the iron spins and to the small coherence length of superconducting pairs. This situation does not exclude a possible influence of the superconductivity on the iron spin dynamics in the paramagnetic state. Such an effect could be evident in a sample in which T_f is well below T_c . In $\text{YBa}_2(\text{Cu}_{0.94}\text{Fe}_{0.6})_3\text{O}_{7-y}$ ($T_f \approx 18$ K and $T_c \approx$

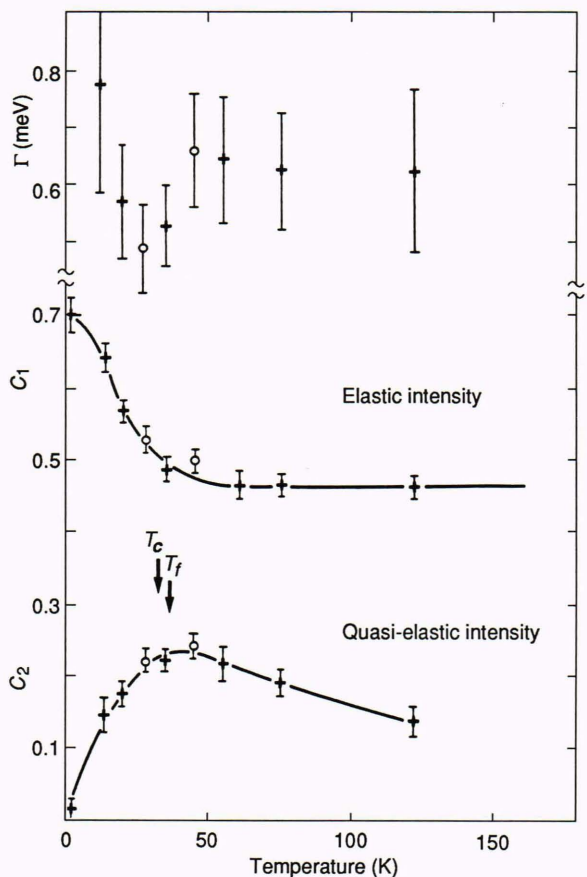


Figure 13. Temperature dependence of the three parameters extracted from the fits. Γ and C_2 are the energy line width and the norm of the Lorentzian function used for the quasi-elastic intensity, respectively, and C_1 is the norm of the delta function used for the “elastic” intensity. Cross symbols (+) correspond to measurements taken with decreasing temperature whereas open symbols (o) correspond to a further increase of temperature. No irreversibility effects are observed during this procedure.

74 K) preliminary TOF results²⁷ indicate some anomalies in the iron spin relaxation above T_f , which could be related to the onset of superconductivity. Detailed measurements and analyses are in progress.

THEORY

We have performed theoretical investigations in order to better understand the electronic structure and properties of the high- T_c superconductors in the normal state, which knowledge is a prerequisite for any realistic challenge to the problem of the superconducting mechanism itself. Of obvious interest are the mobile, charge-carrying holes (these are inherently present in non-stoichiometric $\text{YBa}_2\text{Cu}_3\text{O}_{7-y}$ and are introduced into insulating La_2CuO_4 by alkaline earth doping). The key questions relate to the orbital symmetry of the holes and their degree of coupling to the antiferromagnetic Cu^{2+} (3d) spin system. Our analysis has emphasized a crystal field model that regards the oxide superconductors as primarily ionic crystals, wherein the mobile holes move along potential gradients comprised of the ionic crystal

field potential and the atomic potentials of the individual ions.²⁸ This model readily estimates the energies required to place a mobile hole on different ions and also different orbitals within the same ion, which is useful in determining the distribution and mobility of these holes. It is also useful for calculating various quantities involved in interpretation of nuclear magnetic resonance (NMR) experiments such as the electric field gradient tensors at the atomic nuclei of the various ions.²⁹

Analyses of NMR data from other laboratories, such as the shift of the $^{89}\gamma$ NMR frequency³⁰ and the ^{17}O EFG tensors in $\text{YBa}_2\text{Cu}_3\text{O}_7$ (author's notes: Adrian, F. J., "Structural Analysis of ^{17}O in $\text{YBa}_2\text{Cu}_3\text{O}_{7-y}$ "), contribute to a growing chain of evidence indicating that the conduction holes are largely oxygen-like at the Fermi energy level and that their orbital symmetry is the same as, and thus permits mixing with, the Cu^{2+} (3d) spins. This picture is far from complete, however, and needs to be reconciled with other experimental and theoretical findings that exhibit varying degrees of inconsistency with it. Such problems, which reflect the general state of uncertainty and controversy in the study of low- T_c superconductivity, are the subject of intense investigation at APL and many other laboratories. Theoretical computations and conceptual arguments have been presented recently³¹ that indicate that substitution-induced superstructures may play an important role in attaining tetragonal symmetry in a broad class of substituted high- T_c ceramics.

APPLICATIONS

The approach to applications used by APL is to develop simple passive devices, such as detectors of electromagnetic radiation and microwave microstrip components.² More sophisticated active devices, such as tunnel junctions and related devices, await further developments in fabrication technology. The original goal of our applications work has been to develop a practical high-temperature superconductor bolometer that could be tested in lieu of a semiconducting bolometer in a laboratory Fourier transform spectrometer. The hope is that the high-temperature superconductor detector would be at least as sensitive as the pyroelectric detector and cover a broader spectral range extending beyond the long-wave infrared band (8 to 12 μm). Based on recent calculations, this appears to be a realizable goal. Further testing and design work remains to integrate the Bi-Sr-Ca-Cu-O meander-line detection element pictured in Figure 2 with a low-temperature junction field-effect transistor amplifier and a micro-miniature cryogenic refrigerator.

The experimental results of a recent optical detection experiment are shown in Figure 14. The optical response peak is located at the center of the resistive transition region around T_c . From standard bolometric theory, it is known that the bolometric response is proportional to the derivative of the resistance curve. The derivative of the resistance (dR/dT) curve is also shown in Figure 14, below the measured response. It can be seen that the measured data correlates well with the dR/dT plot. Thus it can be assumed that the optical response is primarily bolometric.

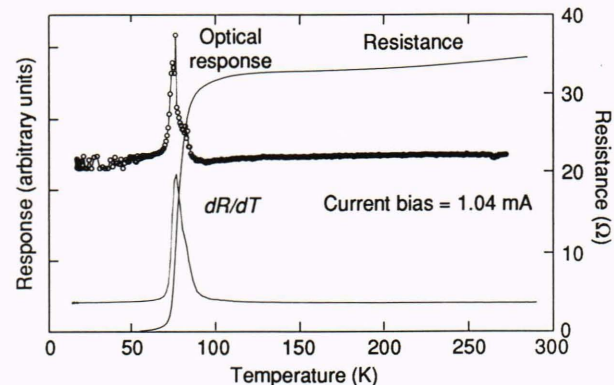


Figure 14. Optical response, resistance, and dR/dT of LAP 10F sample. (Reprinted, with permission, from Ref. 25.)

For microwave detection measurements, shown in Figure 15, a 9-GHz microwave signal was generated with a microwave oscillator and modulated by a 40-Hz square wave with a PIN (p-type/insulating/n-type) diode modulator. The signal was then amplified and fed into an X-band horn. The horn was placed against the cold head window directly in front of the sample used in the optical experiment. As before, the sample was current biased to a fixed value (I_B) with a battery and its response was measured with a lock-in, which is a phase-sensitive detector tuned to the modulation frequency (40 Hz). (The resistance [R] was inferred from the nanovoltmeter measurement [V] using the relationship $R = V/I_B$.) At low microwave power levels (1 to 10 mW measured at the oscillator), the peak of the response varies linearly with microwave power. At higher power levels (50 to 100 mW), however, the response varies nonlinearly with microwave power, indicating that saturation is occurring. Unlike the optical response, the peak in the microwave response is located (in temperature) in the region of the resistive tail well below T_c . This is similar to the weak-link response discussed earlier, though complete understanding requires further experiments, which are now in progress.

The modulated techniques have led to the possibilities of a number of novel devices, for which invention disclosures have been filed. A non-SQUID* vector superconducting magnetometer design operable at 77 K is based on the analysis (confirmed by our experiments) that the component $R(\omega_m)$ of the resistance at the modulation frequency ω_m is linearly dependent on the DC magnetic field, H_{DC} , for $H_{\text{DC}}/H_m \ll 1$, where H_m is the modulation field. This concept therefore forms the basis of a vector magnetometer, since the component of H_{DC} collinear with H_m is measured. Besides this simple magnetic sensor, other sensors have been conceived, depending on the parameter that is modulated. Invention disclosures for an acoustic sensor and a radiation sensor have been filed and modulation of other parameters is under consideration.

*SQUID: Superconducting quantum interference device

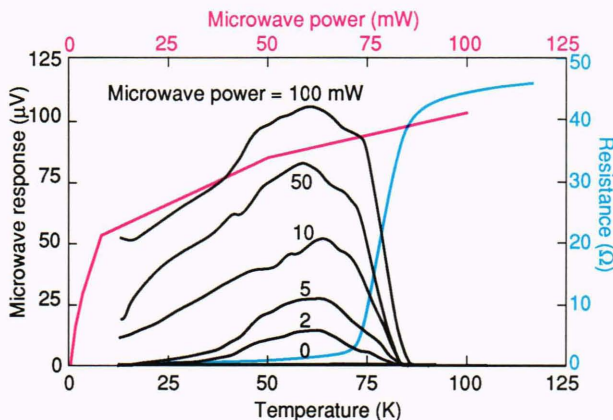


Figure 15. Microwave response versus temperature for the same sample as in Figure 14 for various microwave powers (family of black curves). The corresponding resistance versus temperature curve (blue curve) and the corresponding peak microwave response versus microwave power measured at the oscillator (red curve) are shown as overlays.

SUMMARY

As indicated by this update, developments in high-temperature superconductivity since its inception in early 1987 have altered somewhat the focus of research in this field, but overall activity has diminished only slightly.

Electronics and sensors clearly have greater near-term potential than do applications involving high power transmission or the generation of strong magnetic fields. Accordingly, many laboratories around the world, including APL, have been working toward improved superconducting thin films and better methods of characterizing them. Progress has been rapid, some device prototypes have been constructed, and it is likely that the next update of this field will discuss some working devices.

The mechanism of high- T_c superconductivity has proved to be a formidable problem, and even determining the electronic structure of the CuO₂ planes (which is an essential prerequisite to a realistic challenge to the mechanism problem) has been difficult and controversial. Recent work using semiempirical theory in conjunction with a growing body of reproducible experimental data on well-characterized samples has largely resolved the structure problem and this may lead to a solution of the mechanism problem.

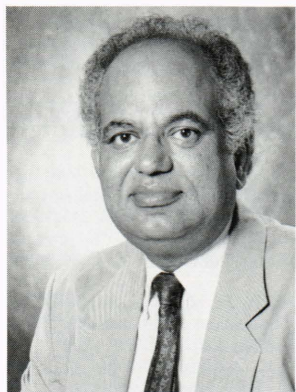
High- T_c superconductivity remains a vibrant field of scientific endeavor. It undoubtedly will enrich science and technology to a significant degree, and is likely to provide revolutionary advances in such areas as novel electronic devices and new physical principles needed to explain the phenomenon.

REFERENCES

- ¹Moorjani, K., "High Temperature Superconductivity," Proc. International Society for Hybrid Microelectronics, Baltimore, p. 15 (1989).
- ²Moorjani, K., Adrian, F. J., Kim, B. F., Bohandy, J., Phillips, T. E., Green, W. J., Agostinelli, E., and Boone, B. G., "High Temperature Superconducting Thin Films," *Johns Hopkins APL Tech. Dig.* **9**, p. 174 (1988).
- ³Moorjani, K., Bohandy, J., Adrian, F. J., Kim, B. F., Shull, R. D., Chiang, C. K., Swartzendruber, L. J., and Bennett, L. H., "Superconductivity in Bulk and Thin Films of La_{1.85} Sr_{0.15} CuO_{4-x} and YBa₂ Cu₃ O_{7-y}," *Phys. Rev. B* **36**, 4036 (1987).
- ⁴Kim, B. F., Bohandy, J., Phillips, T. E., Green, W. J., Agostinelli, E., Adrian, F. J., Moorjani, K., Swartzendruber, L. J., Shull, R. D., Bennett, L. H., and Wallace, J. S., "Superconducting Thin Films of Bi-Sr-Ca-Cu-O Obtained by Laser Ablation Processing," *Appl. Phys. Lett.* **53**, 321 (1988).
- ⁵Bohandy, J., Agostinelli, E., Green, W. J., Phillips, T. E., Kim, B. F., Adrian, F. J., and Moorjani, K., "Laser Ablation Deposition of BiSrCaCuO Thin Films on Zirconia Buffered Crystalline Quartz Substrate," *J. Appl. Phys.* **65**, 4447 (1989).
- ⁶Agostinelli, E., Bohandy, J., Green, W. J., Kim, B. F., Adrian, F. J., and Moorjani, K., "Reduced 'Splashing Effect' in Laser Ablated Superconducting Thin Films Formed from an Amorphous Target," *J. Mater. Res.* (in press).
- ⁷Kim, B. F., Bohandy, J., Moorjani, K., and Adrian, F. J., "A Novel Microwave Technique for Detection of Superconductivity," *J. Appl. Phys.* **63**, 2029 (1988).
- ⁸Moorjani, K., Kim, B. F., Bohandy, J., and Adrian, F. J., "Investigation of High Temperature Superconductivity by the Magnetically Modulated Microwave Absorption Method," *Rev. Solid State Sci.* **2**, 263 (1988).
- ⁹Kim, B. F., Bohandy, J., Adrian, F. J., and Moorjani, K., "A Novel Microwave Technique for Detection of Superconductivity," U.S. Patent 4,851,762 (25 Jul 1989).
- ¹⁰Bohandy, J., Phillips, T. E., Adrian, F. J., Moorjani, K., and Kim, B. F., "Detection of Superconducting Transitions by Magnetically Modulated Electrical Resistance," *Modern Phys. Lett. B* **3**, 933 (1989).
- ¹¹Bohandy, J., Kim, B. F., Phillips, T. E., Adrian, F. J., and Moorjani, K., "A Method for Detection of Weak Links in the Current Path of Electrically Continuous Superconducting Samples," U.S. Patent Application (Mar 1989).
- ¹²Kim, B. F., Bohandy, J., Adrian, F. J., Phillips, T. E., and Moorjani, K., "Magnetically Modulated Resistance Techniques for Studying Thin Film Superconductors," *Proc. ISHM '89 International Society for Hybrid Microelectronics*, Baltimore, p. 47 (1989).
- ¹³Bennett, L. H., Swartzendruber, L. J., Kaiser, D., Bohandy, J., Kim, B. F., Adrian, F. J., and Moorjani, K., "SQUID and MAMMA Observations of the Superconducting Transition in Single Crystals of YBa₂ Cu₃ O_{7-x}," *J. Appl. Phys.* (in press).
- ¹⁴Agostinelli, E., Bohandy, J., Green, W. J., Barger, C. B., Phillips, T. E., Kim, B. F., Adrian, F. J., and Moorjani, K., "Preparation and Characterization of the Superconducting System Bi_{1-x}Pb_xSrCaCu₂O_y," *J. Mater. Res.* **4**, 1103 (1989).
- ¹⁵For example, "Research News," *Science* **244**, pp. 914-916 (1989).
- ¹⁶Dubson, M. A., Herbert, S. T., Calabrese, J. J., Harris, D. C., Patton, B. R., and Garland, J. C., "Non-Ohmic Dissipative Regime in the Superconducting Transition of Polycrystalline Y₁ Ba₂ Cu₃ O_x," *Phys. Rev. Lett.* **60**, 1061-1064 (1988).
- ¹⁷Bohandy, J., Kim, B. F., Adrian, F. J., and Moorjani, K., "Particle Size and Temperature Dependence of Microwave Noise in Superconducting YBa₂ Cu₃ O_{7-y}," *Phys. Rev. B* **39**, 2733 (1989).
- ¹⁸Kim, B. F., Bohandy, J., Phillips, T. E., Adrian, F. J., and Moorjani, K., "Detection of Weak Link Superconductivity by Magnetically Modulated Electrical Resistance," *Physica C* **161**, 76 (1989).
- ¹⁹Deutscher, G., and Müller, K. A., "Origin of Superconductive Glassy State and Extrinsic Critical Currents in High- T_c Oxides," *Phys. Rev. Lett.* **59**, 1745 (1987).
- ²⁰Anderson, P. W., "The Resonating Valence Bond State in La₂ CuO₄ and Superconductivity," *Science* **235**, 1196 (1987).
- ²¹Kistenmacher, T. J., "Substitution for Cu in YBa₂ Cu₃ O₇: the First 3%," *Phys. Rev. B* **38**, 8862 (1988).
- ²²Phillips, T. E., Bohandy, J., and Moorjani, K., "Substitution of Cu by Fe in the Superconducting Ceramic Oxide EuBa₂ Cu₃ O_y: Structure, Electrical Conductivity and Microwave Response," *J. Supercond.* **2**, 305 (1989).
- ²³Moorjani, K., Bohandy, J., Kim, B. F., Adrian, F. J., Du, Y. W., Tang, H., Qiu, Z. Q., and Walker, J. C., "Superconductivity and Spin-Glass Ordering in RBa₂(Cu_{1-x}Fe_x)₃O₇: R = Y, Gd; 0 ≤ x ≤ 0.12," *J. Appl. Phys.* **63**, 4161 (1988).
- ²⁴Kistenmacher, T. J., Bryden, W. A., Morgan, J. S., Moorjani, K., Du, Y. W., Qiu, Z. Q., Tang, H., and Walker, J. C., "Stabilization of the Tetragonal Phase and Superconducting Behavior in RBa₂(Cu_{1-x}Fe_x)₃O_y (R = Y, Gd; 0 ≤ x ≤ 0.15)," *Phys. Rev. B* **36**, 8877 (1987).
- ²⁵Mirebeau, I., Hennion, M., Coddens, G., Phillips, T. E., and Moorjani, K., "Spin Glass Freezing in the Superconducting YBa₂(Cu_{0.88}Fe_{0.12})₃O₇," *Europhys. Lett.* **9**, 181 (1989).
- ²⁶Moorjani, K., and Coey, J. M. D., *Magnetic Glasses*, Elsevier Science Publ., Amsterdam (1984).
- ²⁷Hennion, M., Mirebeau, I., Coddens, G., Menelle, A., Phillips, T. E., Moorjani, K., and Hervieu, M., "Dynamics of Fe in Superconducting YBa₂(Cu_{1-x}Fe_x)₃O_y by Neutron Scattering," *Physica* **159**, 124 (1989).
- ²⁸Adrian, F. J., "Implications of Crystal-field and Intra-atomic Interactions for High- T_c Superconductors," *Phys. Rev. B* **37**, 2326 (1988).

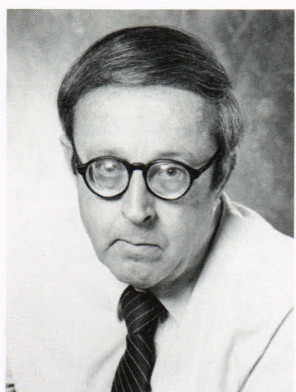
- ²⁹Adrian, F. J., "Structural Implications of Nuclear Electric Quadrupole Splittings in High- T_c Superconductors," *Phys. Rev. B*, **38**, 2426 (1988).
³⁰Adrian, F. J., "Nature of The Conduction Band States in $\text{YBa}_2\text{Cu}_3\text{O}_7$ as Revealed by Its Yttrium Knight Shift," *Phys. Rev. Lett.* **61**, 2148 (1988).
³¹Kistenmacher, T. J., "Substitution-Induced Superstructures in Cu(1)-Doped $\text{YBa}_2\text{Cu}_{1-x}\text{M}_x\text{O}_7$ Ceramics (M = trivalent cation)," *Phys. Rev. B* **39**, 12279 (1989).

THE AUTHORS



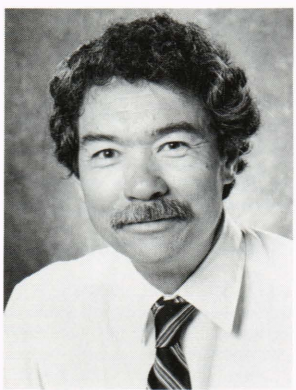
KISHIN MOORJANI is a physicist in the Materials Research Group of APL's Milton S. Eisenhower Research Center. He is engaged in problems related to high-temperature superconductors, photon-beam processing of materials, disordered structures, and nanocomposites. Born in India, he studied at the University of Delhi before receiving a Ph.D. in theoretical physics from The Catholic University of America in 1964. In 1967, Dr. Moorjani joined APL, where he is program manager of the microphysics project. He has coauthored a monograph, *Magnetic Glasses*, and has

published extensively in the field of condensed matter science. He has held several visiting appointments at universities both in the United States and abroad. Dr. Moorjani teaches at The Johns Hopkins University G.W.C. Whiting School of Engineering and serves as chairman of the University's Applied Physics Program Committee.

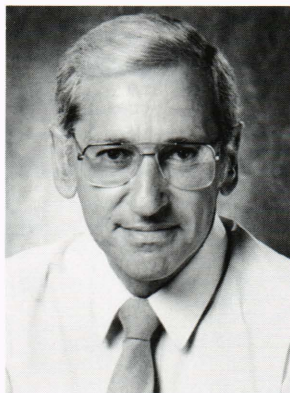


FRANK J. ADRIAN is a member of the Principal Professional Staff and is a senior scientist in APL's Milton S. Eisenhower Research Center. He joined the Research Center in 1955 after receiving an A.B. degree in chemistry from The Catholic University of America (1951) and a Ph.D. degree in physical chemistry from Cornell University (1955). His primary research interests are theoretical and experimental investigations of the structure of molecules and solids and the relationships between structure and chemical and physical properties. Many of these investigations, which have resulted

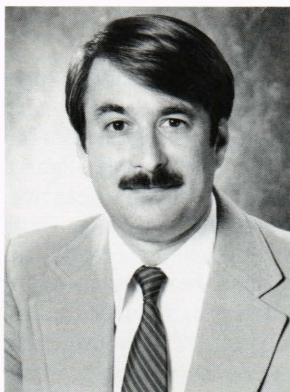
in numerous publications, have involved the application and interpretation of magnetic resonance experiments. Dr. Adrian has been a Dunning visiting professor in the Chemistry Department of The Johns Hopkins University (1982-83) and is an adjunct professor in the Chemistry Department of Queen's University, Kingston, Ontario, Canada.



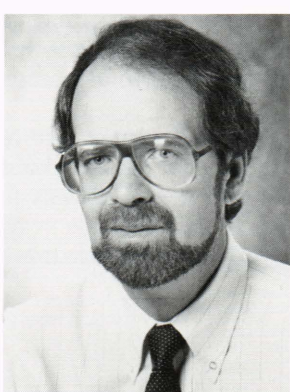
BORIS F. KIM was born in Ashland, Ga., in 1938. He received a B.E.S. degree in electrical engineering in 1960 and a Ph.D. in physics in 1967 from The Johns Hopkins University. Dr. Kim served as an officer in the U.S. Army from 1967 to 1969, after which he joined APL. His research interests are in the fields of experimental atomic and molecular spectroscopy, computer vision, and superconductivity.



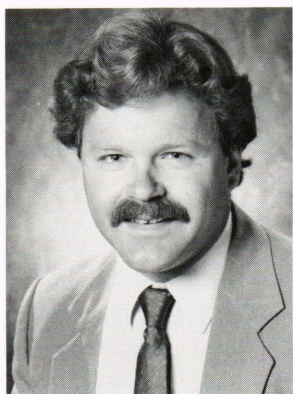
JOSEPH BOHANDY, a native of Ohio, received B.S., M.S., and Ph.D. degrees from Ohio State University. He joined APL in 1965 as a member of the Microwave Physics Group of the Milton S. Eisenhower Research Center and worked on various problems in solid-state and chemical physics. In 1984, he became a member of the Materials Science Group of the Research Center, where he was involved in laser microchemical processing as applied to microcircuit fabrication. His recent principal professional efforts have been in the study and application of high-temperature superconductivity.



TERRY E. PHILLIPS is a senior staff chemist in the Materials Science Group of APL's Milton S. Eisenhower Research Center. Born in Sunbury, Pa., he received a B.A. degree from Susquehanna University, and M.S. and Ph.D. degrees in chemistry from The Johns Hopkins University in 1976. After completing postgraduate studies at Northwestern University in low-dimensional organic conductors, he joined APL in 1979. Dr. Phillips has been involved in problems in photoelectrochemical energy conversion, inorganic optical and electrical phase transition compounds, superconducting materials, and materials characterized with X rays, nuclear magnetic resonance, mass spectroscopy, and optical spectroscopic techniques.



THOMAS J. KISTENMACHER is a Principal Professional Staff chemist in APL's Milton S. Eisenhower Research Center. He obtained a B.S. degree in chemistry from Iowa State University and M.S. and Ph.D. degrees in chemistry from the University of Illinois. During 1969-71, he was a Junior Fellow in chemical physics at the California Institute of Technology. During 1971-82, he served on the faculties of The Johns Hopkins University and the California Institute of Technology. Dr. Kistenmacher joined APL in 1982 as a member of the Microwave Physics Group. In 1984, he became a member of the Materials Science Group, where his current research interests include crystalline structure and structure-physical property relationships in highly conductive organic solids, local structure and magnetic properties of amorphous thin films and multilayers, the elucidation of structural models for icosahedral materials, the structural basis for high- T_c oxide ceramics, and large bandgap metal-nitride semiconductors.

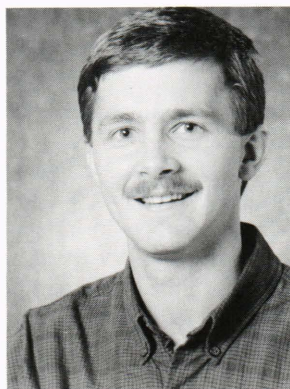


WILLIAM J. GREEN was born in Bethesda, Md., in 1957. He attended both Gettysburg College and the University of Maryland and plans to pursue a degree in applied physics at The Johns Hopkins University G.W.C. Whiting School of Engineering. Before joining the Micro-physics Group of APL's Milton S. Eisenhower Research Center in 1985, he worked for Fusion Systems, Inc., of Rockville, Md., in quality assurance spectroscopy for ultraviolet curing systems. He also worked on a refractometer project for the Quantum Electronics Group at the University of Maryland.



ELISABETTA AGOSTINELLI was born in Gubbio, Italy, in 1956. She received the title of Doctor of Chemistry *cum laude* in 1982 from the University of Rome, where her thesis was on solid-state physics. She joined the Institute of the National Research Council of Italy in Rome on a fellowship, where she was involved in various problems of solid-state physical chemistry. In 1984, she became a researcher and started to study the magnetic properties of spin glasses and amorphous materials. In 1987, she was sponsored for a NATO fellowship by the Microphysics Group of APL's Milton S. Eisenhower Research Center and joined the program on the preparation and characterization of thin films of superconducting oxides.

BRADLEY G. BOONE's biography can be found on p. 35.



RAYMOND M. SOVA received a B.S. degree in electrical engineering from the Pennsylvania State University in 1986. He is pursuing a M.S. degree in applied physics from The Johns Hopkins University Evening College. He is a member of APL's Electro-optical Systems Group, where he is currently working on the development of high-temperature superconducting thin-film devices and the analysis of an infrared seeker system.